Heavy-Cargo Mars Mission Using Near-Term Technology

IEPC-2017-598

Presented at the 35th International Electric Propulsion Conference
Georgia Institute of Technology – Atlanta, Georgia – USA
October 8–12, 2017

William J. Coogan* and Pierre-Yves C. R. Taunay*
Princeton University, Princeton, NJ, 08544, USA

A heavy-cargo mission to Mars is investigated to determine the maximum deliverable payload using electric propulsion. In contrast to previous analyses, this work assumes the use of contemporary technology. The spacecraft trajectory is composed of three segments—one at low-Earth orbit and two in the heliocentric frame. The total payload mass is maximized as a function of thrust steering angle and thrust and coast durations. This electric propulsion mission is compared to a similar chemical propulsion mission; both start at low-Earth orbit with an initial mass of 23 metric tons. In the range of 100 to 400 kW of input power, the travel time for electric propulsion is found to be 1.4 to 2.8 times longer than that for chemical propulsion. Depending on whether or not the power supply is included in the payload, the electric propulsion mission delivers a maximum of 1.9 to 2.5 times the mass deliverable by chemical propulsion.

Nomenclature

a	Semi-major axis length, m	*Subscripts*	
e	Orbital eccentricity		
g_0	Gravitational constant at sea level, m/s^2	avg	Average
I_{sp}	Specific impulse, s	chem	Chemical
m	Mass, kg	LEO	Low-Earth orbit
$\dot{m}$	Mass flow rate, kg/s	nom	Nominal
P	Power, W	payload	Payload
r	Radial distance, m	prop	Propellant
T	Thrust, N	PS	Power supply
u_{e}	Exhaust velocity, m/s	T	Thruster
v	Velocity, m/s	$\oplus$	Earth
α	Specific mass, kg/kW	$\male$	Mars
γ	Thrust angle, degrees	$\odot$	Sun
θ	Azimuthal angular coordinate, degrees	∞	Sphere of influence of Earth
μ	Gravitational parameter, m^3/s^2		

I. Introduction

Electric propulsion has been promoted as a technology capable of bringing crews and their payloads to Mars with considerable mass savings compared to similar missions employing chemical propulsion.[1–6] To achieve a similar transit time to chemical propulsion missions and a larger delivered payload mass, electric propulsion missions require low-specific-mass power supplies, along with high-power thrust systems (greater than 100 kW).[2] Numerous studies[1–6] have investigated such electric propulsion missions. However, many of these studies assume currently unrealistic power supply characteristics. Specific masses are an order of

*Graduate Student, MAE Dept., Princeton University, AIAA Student Member.

magnitude lower than presently available[1–5] and missions require orders of magnitude more power than presently achievable.[1–6] While these assumptions about power supply characteristics may hold at a future date, they currently underpredict transfer times to Mars and inflate the total amount of payload mass that can be delivered.

Our goal is to determine the most near-term capabilities of an electric propulsion spacecraft for a mission to Mars using 100 to 400 kW of power. We simulate this mission using characteristics of the most state-of-the-art technologies presently available in terms of launch vehicles, electric thrusters, and space-based power supplies. This mission features a thrust-coast-thrust engine sequence which minimizes the propellant mass required to match the orbit of Mars as a function of thrust and coast time and thrust steering angle. We develop a trajectory analysis tool to obtain the total delivered payload mass and the total transfer time. We compare the results of the electric propulsion mission to a similar chemical propulsion mission.

In Sec. II, we assess the state-of-the-art technology for electric and chemical propulsion and power supplies, and present the chosen parameters for our analysis. We delineate the method used to determine the trajectory in Sec. III and describe and validate an optimization strategy to minimize the total propellant mass in Sec. IV. We compare the results of our study to a similar mission employing chemical propulsion in Sec. V.

II. Assessment of Current and Near-Term Technologies

A. Launch vehicles and upper stages

The lift capabilities of existing launch vehicles limit the initial mass of our spacecraft. A comparison of the presently operational heavy-lift launch vehicles along with their respective upper stages is given in Table 1. Based on the capabilities listed, we assume that our spacecraft has an initial mass of 23 metric tons (mT) at 400 km above the surface of the Earth. To simplify our analysis, we do not consider Δv penalties resulting from inclination or drag. We apply the parameters of the RL10B-2 engine to the chemical propulsion mission, as it has the largest specific impulse, which results in the smallest propellant mass.

Table 1. Comparison of heavy-lift launch vehicles and respective upper stages.

Vehicle	Delivery orbit	Payload mass (mT)	Upper stage	
			Engine	I_{sp} (s)
Delta IV Heavy[7,8]	200 km, 28.7°	28.8	RL10B-2	465
	407 km, 51.6°	26.0		
Angara A5[9–11]	200 km, 63°	24.0 – 24.5	RD-0146	451–463
Long March 5[12,13]	200×400 km, 42°	23.0	YF-75D	442
Proton-M[14,15]	180 km, 51.5°	23.0	S5.98M	326
Falcon 9[16,17]	N/A	22.8	Merlin 1D	342
Ariane 5[18,19]	260 km, 51.6°	20.0	HM7B	446

B. Electric Propulsion

We assume that we can use an array composed of any number of thrusters to achieve a given power level. The propellant mass flow rate $\dot{m}$ therefore scales linearly with the input power P, such that

$$\dot{m} = \dot{m}_{\text{nom}} \frac{P}{P_{\text{nom}}}, \tag{1}$$

where the subscript nom designates the nominal quantities for the thruster considered.

Table 2 summarizes the commercially available or under-development Hall and ion thrusters. We do not include magnetoplasmadynamic thrusters, VASIMR®, or other advanced concepts in our analysis, as they have a lower technology readiness level (TRL). We seek a high thrust-to-power ratio (T/P) in order to reduce transit time. The HIVHAC is a state-of-the-art thruster that features one of the largest thrust-to-power ratios, as well as a high specific impulse. Although data for higher-power thrusters (e.g. X3 or 457m) are incomplete, specific impulse, thrust-to-power ratio, and specific mass (α_{T}) remain similar. We therefore

assume that high-power, near-term thrusters can be clustered to operate in the range of 100 to 400 kW, and retain the specific impulse and specific mass of the HIVHAC for our calculations.

Table 2. Nominal performance data for high-power electric thrusters.

Type	Thruster	P (kW)	m (kg)	I_{sp} (s)	$\dot{m}$ (mg/s)	T (mN)	T/P (mN/kW)	α_T (kg/kW)
Hall	BHT-8000[20]	8	25	2,210	20.7	449	56	3.1
	HIVHAC[21]	8	10.4	2,800	15	412	52	1.3
	BHT-20k[22]	15	N/A	2,320	35	797	53	N/A
	SPT-290[23]	30	N/A	3,000	48	1,410	47	N/A
	NASA 457m[24]	40	N/A	2,340	87	2,000	50	N/A
	X3[25]	30–200*	250	1,840	93	1,518	50	1.3 – 8.3
Ion	NEXT[26]	6.9	12.7	4,100	5.9	237	34	1.8
	NEXIS[27]	25	29.1	7,500	6.4	471	19	1.2
	HiPEP[28,29]	39.3	46.5	9,620	7	661	17	1.2

* Though the X3 is rated for 200 kW of input power, published data are only available up to 30 kW.[25]

C. Power supplies

For missions to Mars, available solar arrays have both a higher TRL and a lower specific mass than nuclear fission alternatives.[30–32] We therefore consider only solar power supplies, examples of which are given in Table 3. For our analysis, we assume the specific mass of the power supply of the International Space Station (ISS), 35 kg/kW, as it is the largest supply to have been demonstrated in space. This value includes panels, structure, and power processing unit. We consider the solar arrays to be self-deployable, based on active research on deployment mechanisms. Examples of self-deployable systems include MegaFlex™ by Orbital ATK,[33] Roll-Out Solar Array panels by Deployable Space Systems,[34,35] and telescopic panels.[36] The self-deployable concepts are projected to scale up to 250 kW of power per panel, with specific masses ranging from 7 to 20 kg/kW.

Table 3. Solar panels by mission.

Mission	P at 1 AU (kW)	α_{PS} at 1 AU (kg/kW)	Area (m^2)
ISS[31,37]	120	35	2,500
Juno[31]	14	24	60
Dawn[31,38]	10	12.5	38

III. Trajectory Determination

We consider planetocentric and heliocentric trajectories independently. This effectively reduces the computation to a two-body problem over multiple segments. The trajectory of the spacecraft from low-Earth orbit (LEO) to the sphere of influence (SOI) of Earth constitutes the first segment. The second component of the trajectory is in the heliocentric frame, from the SOI of Earth to the SOI of Mars. Any remaining difference in velocity between the spacecraft and Mars at the SOI of Mars is resolved with a final segment using chemical propulsion. In all cases, we assume planar trajectories.

The thrust sequence implemented depends on the type of propulsion considered. The electric propulsion engine fires continuously from LEO until it reaches the SOI of Earth. The final mass and velocity at the SOI may be optimized as a function of the thrust steering angle in this segment. A thrust-coast-thrust engine sequence that minimizes the final Δv to match the velocity of Mars as a function of thrust and coast durations is used in the heliocentric frame. We compute the trajectory through numerical integration of the equations of motion using an implicit Euler method of order 2. This method is a compromise between

stability, accuracy, and computation time. For the chemical rocket, a Hohmann transfer is used to simulate the trajectory, with one impulse at LEO, and one impulse at destination to match the velocity of Mars.

A. Electric propulsion trajectory

1. Equations of motion

The state vector is defined as $\mathbf{x} = \left[r, \theta, m_{\text{prop}}, \dot{r}, \dot{\theta}\right]$, where r and θ define the position of the spacecraft in polar coordinates, and m_{prop} is the amount of propellant spent at any given time. The equations of motion are given by

$$\begin{cases} \dot{r} = \dot{r}, \\ \dot{\theta} = \dot{\theta}, \\ \dot{m}_{\text{prop}} = \dot{m}, \\ \ddot{r} = r\dot{\theta}^2 - \dfrac{\mu}{r^2} + \dfrac{T}{m_0 - m_{\text{prop}}} \sin\gamma, \text{ and} \\ \ddot{\theta} = \dfrac{1}{r}\left(-2\dot{r}\dot{\theta} + \dfrac{T}{m_0 - m_{\text{prop}}} \cos\gamma\right), \end{cases} \tag{2}$$

where γ is the thrust angle with respect to the tangent of a circle of radius r (Fig. 1) and m_0 is the initial mass of the spacecraft.

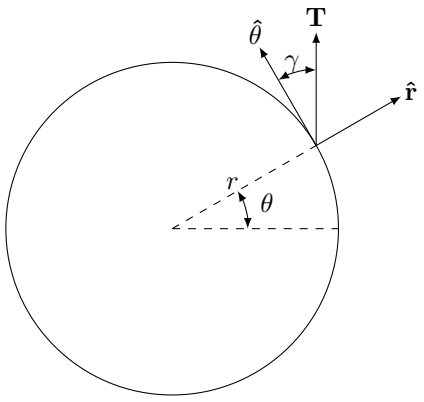

Figure 1. Definition of geometric parameters.

The initial mass of each segment is computed from the final conditions of the previous one. The thrust is defined as

$$T = \dot{m} u_{\text{e}}, \tag{3}$$

where u_{e} is the exhaust velocity. The magnitude of the thrust depends on the power available, which for solar arrays decreases following an inverse-square law with respect to the distance from the Sun, r. At any given distance, the power is

$$P = P_0 \left(\frac{r_\oplus}{r}\right)^2, \tag{4}$$

where $r_\oplus$ is the distance between Earth and the Sun and P_0 is the nominal power at 1 AU. We treat the exhaust velocity as constant and vary $\dot{m}$ as prescribed by Eq. 1.

2. Mission segments

Earth escape: We ignore shading effects and consider constant power. The initial conditions for this segment are $\mathbf{x} = \left[r_{\text{LEO}}, 0, 0, 0, \sqrt{\dfrac{\mu_\oplus}{r_{\text{LEO}}^3}}\right]$, where $\mu_\oplus$ is the gravitational constant of Earth and r_{LEO} is the distance from the center of the Earth to LEO. We solve the differential equations to the point where the spacecraft reaches the sphere of influence ($r = r_\infty$).

Heliocentric trajectory: We assume that the velocity at the SOI of Earth is tangential to the circular orbit of Earth in the heliocentric frame. The initial values are therefore $\mathbf{x} = \left[r_\oplus, 0, 0, 0, \dfrac{v_\oplus + v_\infty}{r_\oplus}\right]$, where $v_\oplus$ is the velocity of Earth in the heliocentric reference frame, and v_∞ is the final velocity achieved in the geocentric frame. We solve the differential equations to the point where the spacecraft is within the sphere of influence of Mars.

We treat the orbits of both Earth and Mars as circular in the heliocentric frame of reference. The radius of each orbit is given by the time-averaged value, defined as

$$r_{\text{avg}} = a\left(1 + \frac{e^2}{2}\right), \tag{5}$$

where a is the semi-major axis of the orbit and e is the eccentricity.

INJECTION INTO THE ORBIT OF MARS: Any remaining Δv required to match the velocity of Mars in the heliocentric frame of reference is eliminated with chemical propulsion. This change in velocity is given by

$$\Delta v_{\mathord{\male}} = \sqrt{(\dot{r}_{2,\mathrm{f}})^2 + \left(r_{2,\mathrm{f}}\,\dot{\theta}_{2,\mathrm{f}} - v_{\mathord{\male}}\right)^2}, \tag{6}$$

where $v_{\mathord{\male}}$ is the velocity of Mars around the Sun and the subscript 2,f designates the final values achieved in the second segment of the trajectory. The rocket equation gives the mass of the propellant spent by this maneuver as

$$m_{\mathrm{prop,chem}} = m_{2,\mathrm{f}}\left[1 - \exp\left(-\frac{\Delta v_{\mathord{\male}}}{g_0 I_{\mathrm{sp}}}\right)\right], \tag{7}$$

where g_0 is the gravitational constant of Earth at sea level.

3. Payload mass

We calculate the total payload mass that can be delivered to Mars using the results of each segment of the trajectory as well as the specific masses of the solar panel system and thruster:

$$m_{\mathrm{payload}} = m_{2,\mathrm{f}} - m_{\mathrm{prop,chem}} - \alpha_{\mathrm{PS}} P_0 - \alpha_{\mathrm{T}} P_0. \tag{8}$$

For simplicity we neglect the mass of the chemical thruster and any additional structural components.

Equation 8 assumes that the power supply is not part of the useful payload. However, almost any conceivable mission requires a power source at its destination. In this case, the power supply can be considered an integral part of the payload. In Sec. V, we independently evaluate the cases where the power supply mass is or is not included in the payload.

B. Chemical Propulsion Trajectory

We model the trajectory of the chemical rocket with a Hohmann transfer in order to maximize the payload mass fraction. The Hohmann transfer consists of two engine impulses. The propellant mass fraction for each impulsive maneuver can be found using Eq. 7 with the appropriate initial mass and Δv.

The first impulse is applied at LEO, resulting in a hyperbolic trajectory in the frame of the Earth, as is illustrated in Fig. 2. The velocity achieved at the sphere of influence of Earth such that the spacecraft reaches Mars at aphelion is given by[39]

$$v_\infty = \sqrt{\frac{\mu_\odot}{r_\oplus}}\left(\sqrt{\frac{2r_{\mathord{\male}}}{r_\oplus + r_{\mathord{\male}}}} - 1\right), \tag{9}$$

where $\mu_\odot$ is the gravitational constant of the Sun, and $r_{\mathord{\male}}$ is the distance between Mars and the Sun. The change in velocity at LEO needed to attain v_∞ is given in Ref. 39 as

$$\Delta v_1 = \sqrt{v_\infty^2 + \frac{2\mu_\oplus}{r_{\mathrm{LEO}}}} - v_{\mathrm{LEO}}, \tag{10}$$

where $v_{\mathrm{LEO}} = \sqrt{\dfrac{\mu_\oplus}{r_{\mathrm{LEO}}}}$.

The second impulse is applied at $r = r_{\mathord{\male}}$ in order to attain a circular final orbit. This requires a change in velocity,[39]

$$\Delta v_2 = \sqrt{\frac{\mu_\odot}{r_{\mathord{\male}}}}\left(1 - \sqrt{\frac{2r_\oplus}{r_\oplus + r_{\mathord{\male}}}}\right). \tag{11}$$

IV. Optimization

A. Thrust angle

The thrust angle affects multiple parameters, such as the amount of propellant and total time spent in a given segment of the trajectory. An arbitrary function that maps values of r to the interval $[0, \pi/2]$ can be

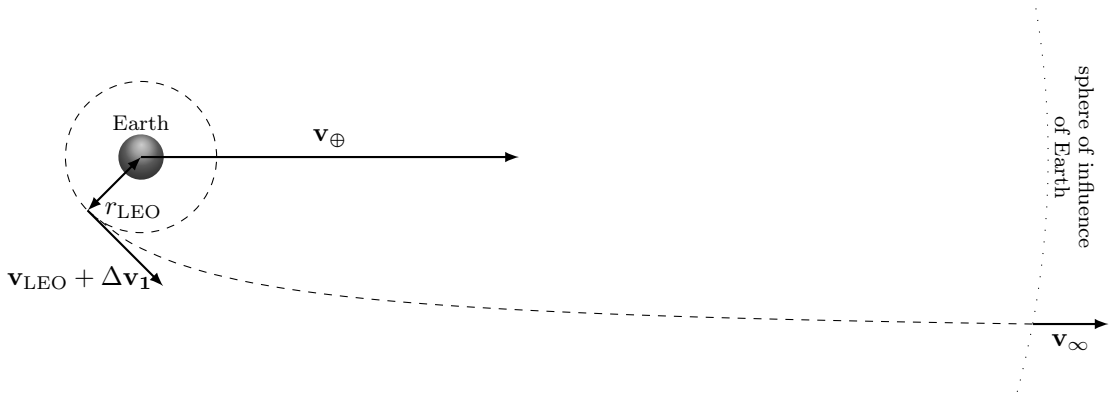

Figure 2. Hyperbolic escape trajectory for chemical propulsion missions.

used to model the variation of the angle as a function of the position. We use the expression

$$\gamma(r) = \frac{\pi}{2} \tanh\left(\sum_{k=0}^{N} \gamma_k \left(r - r_{\mathrm{LEO}}\right)^k\right), \tag{12}$$

where $\gamma_0 = 0$, such that $\gamma(r_{\mathrm{LEO}}) = 0$. The coefficients of the polynomial, γ_k, are the optimization variables. The cost function is the total propellant mass for a segment of the trajectory. We use Scipy's `minimize` function configured with the Nelder-Mead[40] algorithm to compute the optimization variables.

We demonstrate the validity of this approach on the case shown in Ref. 41, using a polynomial of order 3, and compare our results to those of Tang and Conway who use 81 optimization variables. In this comparison, each algorithm minimizes the total transit time from geosynchronous orbit (GEO) to the sphere of influence of Earth. Results are shown in Fig. 3. We obtain good agreement with the optimization results of Tang and Conway.

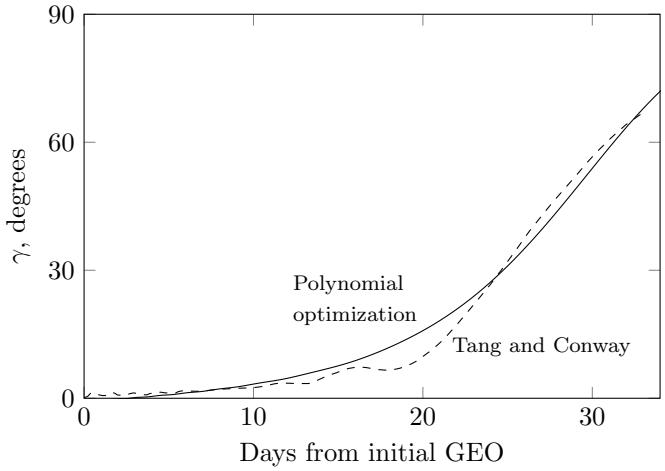

Figure 3. Comparison of polynomial optimization to the results of Tang and Conway.[41]

B. Thrust-coast-thrust engine sequence

The cost function for this trajectory optimization is the total propellant mass fraction for the heliocentric trajectory. The optimization variables are the thrust time for the first engine sequence and the subsequent coast time. With the choice of appropriate initial values, no constraints are needed for the optimization

variables. As with the thrust angle optimization, we use Scipy's `minimize` function configured with the Nelder-Mead[40] algorithm to compute the optimization variables.

The initial guess for the thrust and coast times is found with a first optimization routine. The goal of this routine is to find the minimum amount of propellant that allows the spacecraft to reach Mars on a thrust-coast sequence, with no injection into the orbit of Mars (effectively a fly-by mission). The initial values for the thrust-coast-thrust engine sequence are determined by halving the coasting time found in the first optimization routine, while keeping the duration of the first thrust sequence identical.

V. Results and Analysis

Typical trajectories for the escape from Earth and the heliocentric segments of the mission are shown in Fig 4. We found that in the power range investigated, the variation of the optimal thrust angle was only significant for the geocentric segment of the mission, and within the range reported in Ref. 42 for the heliocentric segment. However, the final payload mass fraction and total mission duration varied by less than 2% with the optimized thrust steering angle, as compared to the case where $\gamma = 0$. We found that a reduction in time spent firing prior to passing the SOI also reduces the velocity at which the spacecraft exits the SOI. Consequently, there is a corresponding increase in time spent firing in the second segment of the mission, resulting in a nearly constant total propellant mass. In light of these results, we set $\gamma = 0$ for all segments of the mission in order to investigate a larger array of power levels in a similar amount of computation time.

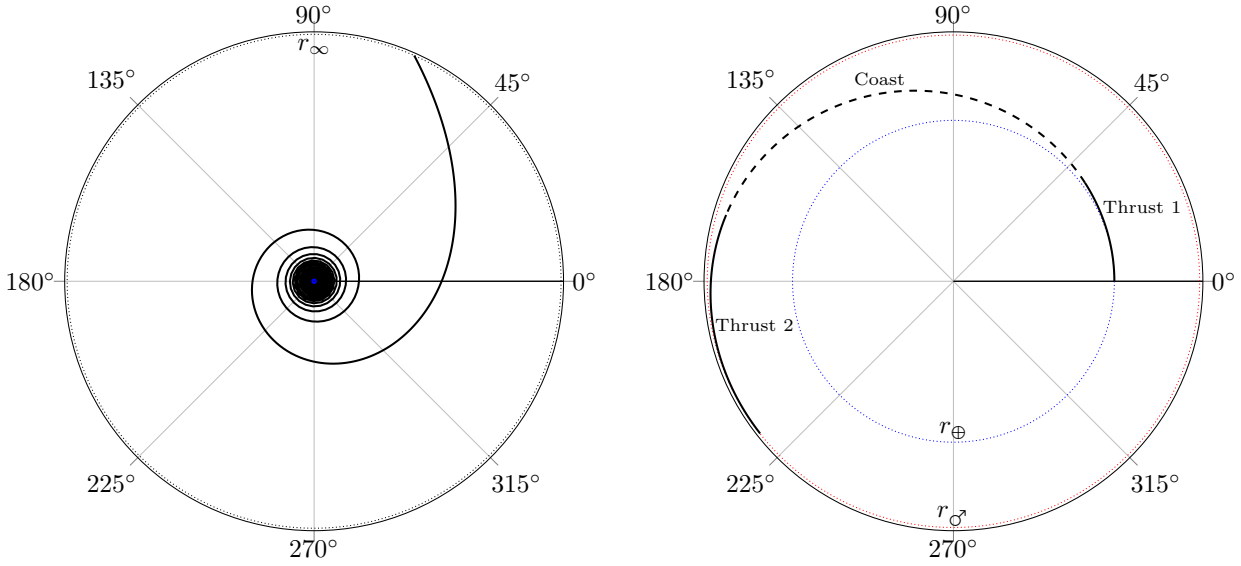

Figure 4. Typical trajectory for Earth escape (left) and travel to Mars (right).

A. Escape from Earth

The propellant mass fraction, time to the SOI of Earth, and velocity at the SOI of Earth are shown in Fig. 5. While electric propulsion leaves the SOI of Earth with a much lower propellant mass fraction, the time spent in the vicinity of Earth is orders of magnitude longer. However, increasing power results in both a rapid decrease in time to reach the SOI and an increase in velocity at the SOI.

B. Heliocentric trajectory

The total time to reach Mars and total payload mass that can be delivered are shown in Fig. 6. For a 23 mT initial mass, chemical propulsion can deliver a total payload mass of 6.0 mT (26% payload mass fraction) with a total travel time of 8.5 months. Results for electric propulsion vary with power, with a maximum delivered mass of 11.2 mT (49% payload mass fraction) if we exclude the power supply. The total transit

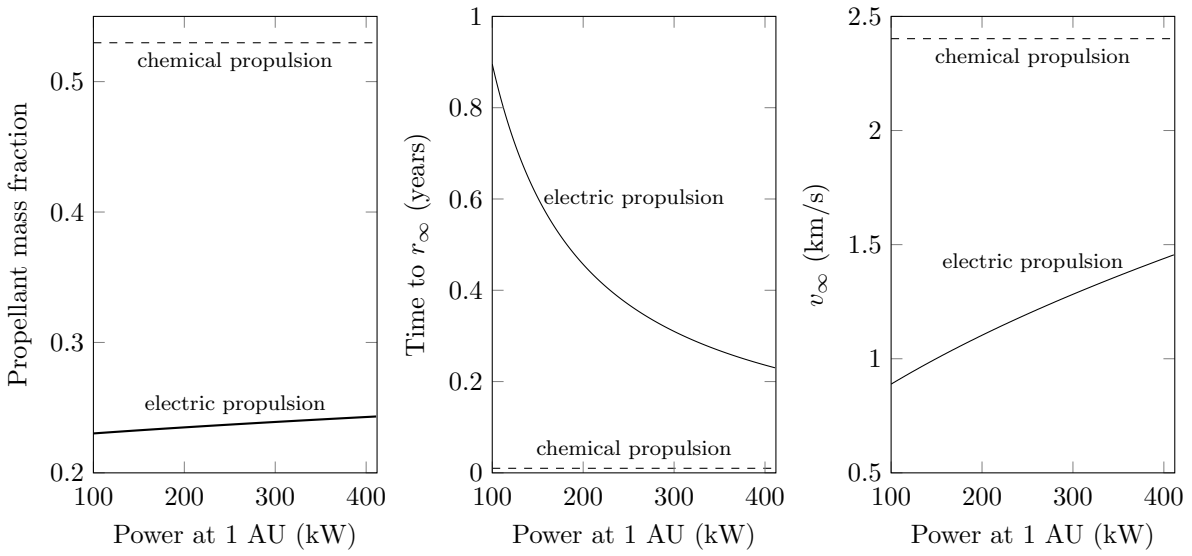

Figure 5. Left: amount of propellant used as a fraction of the total mass when the SOI of Earth is reached. Center: time to reach the SOI of Earth. Right: velocity at SOI of Earth in the geocentric reference frame.

time decreases as power increases, and asymptotes to the duration of a Hohmann transfer. The primary source of the variation in travel time is the duration of the first segment of the mission.

The total payload mass delivered shows a decreasing linear trend with increasing power. Above 411 kW, no payload may be delivered. However, for missions requiring solar electric power at the orbit of Mars, the total delivered mass increases to a range of 13.6 to 14.7 mT (59 to 64% payload mass fraction). In comparison, the 6.0 mT payload delivered by a chemical propulsion mission corresponds to the mass of a 171 kW power supply.

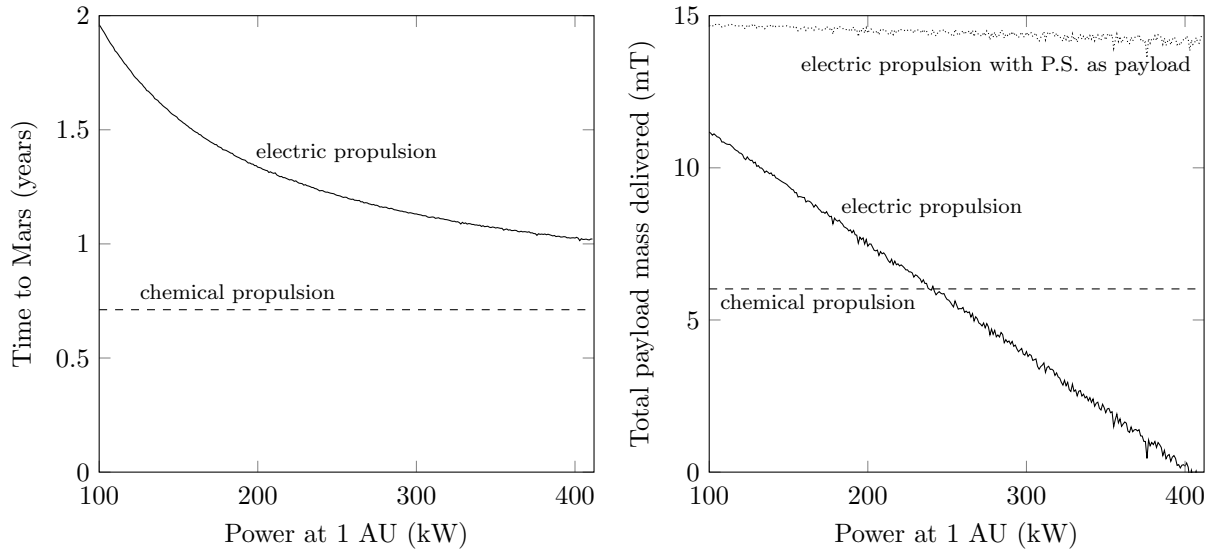

Figure 6. Total travel time to Mars (left) and payload mass delivered (right) for electric and chemical propulsion as a function of solar power at 1 AU.

VI. Conclusion

We simulated Earth-to-Mars trajectories of a spacecraft propelled by solar electric propulsion using parameters for existing and near-term technologies. We computed the thrust steering angle for the geocentric trajectory and the thrust and coasting durations for the heliocentric trajectory that minimize the total amount of propellant spent for a thrust-coast-thrust mission as a function of input power. We found that the thrust steering angle has a negligible impact on the overall performance for the power range investigated.

We compared the results of the electric propulsion mission to a similar chemical propulsion mission that uses a Hohmann transfer to reach Mars. We showed that chemical propulsion always results in shorter mission durations for the mass and power range investigated. However, the durations of electric propulsion missions are of a similar order of magnitude, and are able to deliver a substantially larger payload in most instances.

We showed that electric propulsion is especially suited to missions requiring a large power supply at the orbit of Mars. For such missions the payload mass fraction is found to be as high as 64%, compared to 26% for a high-performance chemical thruster with identical initial conditions. Electric propulsion missions can deliver solar arrays generating as much as 411 kW at 1 AU (176 kW at Mars), whereas existing chemical propulsion systems cannot deliver a solar array generating more than 171 kW (73 kW at Mars).

References

[1]A. V. Ilin, L. D. Cassady, T. W. Glover, and F. R. Chiang Diaz. VASIMR® human mission to Mars. *Space Propulsion and Energy Sciences International Forum*, 2011.

[2]K. Sankaran, L. Cassady, A. D. Kodys, and E. Y. Choueiri. A survey of propulsion options for cargo and piloted missions to mars. *International Conference on New Trends in Astrodynamics*, 2003.

[3]J. H. Gilland, R. M. Myers, and M. J. Patterson. Multimegawatt electric propulsion system design considerations. *AIAA/DGLR/JSASS 21st International Electric Propulsion Conference*, 1990. doi:10.2514/6.1990-2552.

[4]J. W. Dankanich, B. Vondra, and A. V. Ilin. Fast transits to Mars using electric propulsion. *46th AIAA/ASME/SAE/ASEE Joint Propulsion Conference and Exhibit*, 2010. doi:10.2514/6.2010-6771.

[5]H. Youssef and A. Jakubowski. Solar electric propulsion cargo spacecraft for Mars missions. *Aircraft Design and Operations Meeting*, 1991. doi:10.2514/6.1991-3130.

[6]R. H. Frisbee and N. J. Hoffman. Electric propulsion options for Mars cargo missions. *32nd AIAA/ASME/SAE/ASEE Joint Propulsion Conference and Exhibit*, 1996. doi:10.2514/6.1996-3173.

[7]United Launch Alliance. Atlas V and Delta IV technical summary, 2013. URL: http://www.ulalaunch.com/uploads/docs/Launch_Vehicles/AV_DIV_product_card.pdf.

[8]Aerojet Rocketdyne. RL10 engine, Accessed July 2017. URL: http://www.rocket.com/rl10-engine.

[9]The State Space Scientific-Production Center of Khrunichev. Angara launch vehicles family, Accessed July 2017. URL: http://www.khrunichev.ru/main.php?id=44.

[10]I. I. Kuznetsov. *Handbook of Space Security*, chapter Russian Space Launch Programs. Springer, 2015.

[11]V. Rachuk and N. Titkov. The first Russian LOX-LH2 expander cycle LRE: RD0146. *42nd AIAA/ASME/SAE/ASEE Joint Propulsion Conference and Exhibit*, 2006.

[12]M. Xiang and L. Tongyu. The new generation launch vehicles in china. *54th International Astronautical Congress*, 2014.

[13]Z. Nan. The development of LOX/LH2 engine in china. *64th International Astronautical Congress*, 2013.

[14]ILS. Proton launch system mission planner's guide: Section 2. 2009.

[15]Eurockot. Rockot user's guide. 2011. URL: http://www.eurockot.com/wp-content/uploads/2012/10/UsersGuideIss5Rev0web.pdf.

[16]SpaceX. Capabilities and services, Accessed June 2017. URL: http://www.spacex.com/about/capabilities.

[17]SpaceX. Falcon 9 overview, 2013. Internet Archive snapshot of 2013/07/15. URL: http://www.spacex.com/falcon9#merlin_engine.

[18]Arianespace. Technical overview: Ariane 5, Accessed June 2017. URL: http://www.arianespace.com/wp-content/uploads/2015/10/Ariane5_Brochure_Nov2016.pdf.

[19]Snecma-Safran. HM7B brochure, 2013. URL: http://www.snecma.com/IMG/files/fiche_hm7b_ang_2011_modulvoir_file_fr.pdf.

[20]Busek Co. Inc. BHT-8000 Busek Hall Effect Thruster. 2016.

[21]D. T. Jacobson, D. H. Manzellat, R. R. Hofer, and P. Y. Petersen. NASA's 2004 Hall thruster program. *40th AIAA/ASME/SAE/ASEE Joint Propulsion Conference and Exhibit*, 2004. doi:10.2514/6.2004-3600.

[22]Busek Co. Inc. Busek High Power Hall Thruster. 2013.

[23]V. Kim, G. Popov, B. Arkhipov, V. Murashko, O. Gorshkov, A. Koroteyev, V. Garkusha, A. Senekin, and S. Tverdokhlebov. Electric propulsion activity in Russia. *27th International Electric Propulsion Conference*, 2001.

[24]G. C. Soulas, T. W. Haag, D. A. Herman, W. H. Huang, H. Kamhawi, and R. Shastry. Performance test results of the NASA-457M v2 Hall thruster. *48th AIAA/ASME/SAE/ASEE Joint Propulsion Conference and Exhibit*, 2012.

[25]S. J. Hall, S. E. Cusson, and A. D. Gallimore. 30-kW performance of a 100-kW class nested-channel Hall thruster. *34th International Electric Propulsion Conference*, 2015.

[26]M. J. Patterson and S. W. Benson. NEXT ion propulsion system development status and performance. *43rd AIAA/ASME/SAE/ASEE Joint Propulsion Conference and Exhibit*, 2007. doi:10.2514/6.2007-5199.

[27]J. S. Snyder, D. M. Goebel, J. E. Polk, A. C. Schneider, and A. Sengupta. Results of a 2000-hour wear test of the NEXIS ion engine. *29th International Electric Propulsion Conference*, 2005.

[28]D. Fiehler, R. Dougherty, and D. Manzella. Electric propulsion system modeling for the proposed Prometheus 1 mission. *41st AIAA/ASME/SAE/ASEE Joint Propulsion Conference and Exhibit*, 2005. doi:10.2514/6.2005-3891.

[29]J. E. Foster, T. Haag, H. Kamhawi, M. Patterson, S. Malone, F. Elliot, G. J. Williams Jr., J. S. Sovey, and C. Carpenter. The high power electric propulsion (HiPEP) ion thruster. *40th AIAA/ASME/SAE/ASEE Joint Propulsion Conference and Exhibit*, 2004. doi:10.2514/6.2004-3812.

[30]NASA. NASA technology roadmaps, TA 3: Space power and energy storage. Technical report, 2015.

[31]P. Beauchamp, R. Ewell, E. Brandon, and R. Surampudi. Solar power and energy storage for planetary missions. *Presentation*, 2015. URL: http://www.lpi.usra.edu/opag/meetings/aug2015/presentations/day-2/11_beauchamp.pdf.

[32]J. Graham, V. Ionkin, and N. N. Ponomarev-Stepnoi. The role of nuclear power and nuclear propulsion in the peaceful exploration of space. Technical report, International Atomic Energy Agency, 2005.

[33]Orbital ATK. UltraFlex^{TM} solar array systems, 2015. URL: https://www.orbitalatk.com/space-systems/space-components/solar-arrays/docs/fs007_15_oa_3862%20ultraflex.pdf.

[34]NASA. Advanced solar array systems, Accessed June 2017. URL: https://www.nasa.gov/offices/oct/home/feature_sas.html.

[35]Deployable Space Systems. Rosa flight demonstration hardware successfully deploys on iss, Accessed July 2017. URL: http://www.dss-space.com/post/rosa-flight-demonstration-hardware-successfully-deploys-on-iss.

[36]M. Mikulas, R. Pappa, J. Warren, and G. Rose. Telescoping solar array concept for achieving high packaging efficiency. *2nd AIAA Spacecraft Structures Conference*, 2015. doi:10.2514/6.2015-1398.

[37]NASA. International space station solar arrays. Accessed June 2017. URL: https://www.nasa.gov/mission_pages/station/structure/elements/solar_arrays.html#.WW_PQoqQxhE.

[38]NASA. Dawn launch mission to Vesta and Ceres. *Press kit*, 2007. URL: https://www.jpl.nasa.gov/news/press_kits/dawn-launch.pdf.

[39]R. R. Bate, D. D. Miller, and J. E. White. *Fundamentals of Astrodynamics*, chapter 3, 8, pages 163–170, 368–374. Dover Publications, Inc., Mineola, NY, 1971.

[40]J. A. Nelder and R. Mead. A simplex method for function minimization. *The Computer Journal*, 7:308–313, 1965.

[41]S. Tang and B. A. Conway. Optimization of low-thrust interplanetary trajectories using collocation and nonlinear programming. *Journal of Guidance, Control, and Dynamics*, 18, 1995. doi:10.2514/321429.

[42]C. Kluever. Efficient computation of optimal interplanetary trajectories using solar electric propulsion. *Journal of Guidance, Control, and Dynamics*, 38, 2015.